

# Highly mesoporous carbon flakes derived from a tubular biomass for high power electrochemical energy storage in organic electrolyte



Zhimin Zou<sup>a,b</sup>, Tao Liu<sup>a</sup>, Chunhai Jiang<sup>a,\*</sup>

<sup>a</sup> Fujian Provincial Key Laboratory of Functional Materials and Applications, Institute of Advanced Energy Materials, School of Materials Science and Engineering, Xiamen University of Technology, 600 Ligong Road, Jimei District, Xiamen 361024, China

<sup>b</sup> Key Laboratory of Environmental Biotechnology (XMUT), Fujian Province University, 600 Ligong Road, Jimei District, Xiamen 361024, China

## HIGHLIGHTS

- Highly mesoporous carbon flakes were prepared from tubular-structured kapok fibers.
- High mesoporous volumetric ratio of 97.6% towards a pore volume of  $2.756 \text{ cm}^3 \text{ g}^{-1}$  was achieved.
- A low-temperature pre-carbonization in air was effective to dewax the kapok fibers.
- The HMCFs exhibited high energy storage capacitance in organic electrolyte.

## ARTICLE INFO

**Keywords:**  
Supercapacitors  
EDLCs  
Kapok fibers  
Electrode  
Biomass-derived carbons

## ABSTRACT

Carbon flakes with a specific surface area of  $3010 \text{ m}^2 \text{ g}^{-1}$ , a pore volume of  $2.756 \text{ cm}^3 \text{ g}^{-1}$  and an ultrahigh mesoporous volumetric ratio of 97.6% were prepared from tubular kapok fibers through a simple low-temperature pre-carbonization and KOH activation process. The low-temperature pre-carbonization in air was effectively dewaxed the biomass and the thus obtained thin precursor was adequately wetted and etched by KOH, both of which might have resulted in the much improved textural properties. When used as electrode materials of symmetric supercapacitors in organic electrolyte, the carbon flakes displayed high energy density at high power density, e.g.  $24 \text{ Wh kg}^{-1}$  at  $24,029 \text{ W kg}^{-1}$ , which was among the best values reported so far on biomass-derived porous carbon electrodes. The results reported in this work indicated that both the selection of bio-resources and pre-carbonization treatment were important for preparation of carbonaceous electrode materials with tailored texture properties and enhanced electrochemical energy storage performance.

## 1. Introduction

Electrical double-layer capacitors (EDLCs), also referred to supercapacitors, store energy through formation of an electrical double layer of electrolyte ions on the surface of electrode [1–3]. As this energy storage process is majorly controlled by the fast sorption and desorption of electrolyte ions driven by an electric field, EDLCs can be charged and discharged at a much higher rate and with much longer lifetime as compared to secondary batteries. Therefore, EDLCs are widely used in buses, trains, elevators and UPS for regenerative braking, short-term energy storage, burst-mode power delivery or emergency power backup where high power and long lifespan are required [2].

According to the formula  $E = 0.5CV^2$ , the energy density of EDLCs depends on both the operating voltage and the specific capacitance of

the electrode/electrolyte system. The former is mainly determined by the type of electrolyte used, whereas the latter is directly related to the specific surface area (SSA) accessible by the electrolyte ions. For this reason, exploring electrode materials with high SSA and reasonable pore size distribution is recognized as one of the major ways in improving the energy density of EDLCs. Activated carbons are currently the dominating electrode active masses of EDLCs based on their high SSA, enriched microporous structure, high electrical conductivity, and environmentally friendliness [2,4]. However, commercial activated carbons are usually micrometer-scale irregular particles with high portion of micropores. A large part of the microporous surface area of activated carbons is inaccessible to the electrolyte ions (especially for organic electrolyte), which subsequently causes higher inner resistance in the electrode and impedes the charge storage performance of EDLCs [5]. It is commonly accepted that introducing an appropriate

\* Corresponding author.

E-mail address: [chjiang@xmut.edu.cn](mailto:chjiang@xmut.edu.cn) (C. Jiang).

amount of mesopores into the carbonaceous electrode materials may facilitate the transportation of electrolyte ions, thus promote the double layer charge storage [6,7]. In addition, similar to the mostly adopted nanoengineering concept in developing nanostructured electrodes [8], reducing the size of carbon materials in one or two dimensions is also an effective way. For examples, Zhu et al. synthesized a porous carbon with continuous three-dimensional network of highly curved, atom-thick walls by chemically activating the exfoliated graphene oxide. The material showed a high SSA of  $3100 \text{ m}^2 \text{ g}^{-1}$ , high gravimetric capacitance and energy density with organic and ionic liquid electrolytes in two-electrode supercapacitors [9]. Liu et al. showed that a supercapacitor with graphene-based electrodes exhibited a specific energy density of  $85.6 \text{ Wh kg}^{-1}$  at room temperature and  $136 \text{ Wh kg}^{-1}$  at  $80^\circ\text{C}$  (based on the total electrode weight) measured at a current density of  $1 \text{ A g}^{-1}$  [10]. Carbon nanotubes have also been well proven as excellent electrode materials for supercapacitors because of their one-dimensional hollow structure and high electrical conductivity [11].

In addition to graphene and carbon nanotubes, a new class of carbon materials, the so-called biomass-derived carbons, have attracted great interests in recent years due to the abundance, low cost and hierarchical microstructures of the raw materials [12]. Thanks to the broad diversity of natural biomass in macrostructures, mesoporous carbons with various zero to three-dimensional structures have been fabricated [13]. High electrochemical capacitances have been achieved with porous carbons derived from a variety of biomass, such as coconut shell [14], hemp [15], silk [16], corn starch [17], shrimp shells [18], waste coffee grounds [19], lignin [20], algae [21], shaddock skins [22], willow catkins [23], waste tea-leaves [24], rice husk [25], kapok fibers [26], etc. Among the biomass employed, the tubular kapok fibers (KF) can be pyrolyzed or activated to produce nitrogen-doped porous carbons. For examples, Xu et al. fabricated porous carbon nanoflakes with a SSA of  $1635 \text{ m}^2 \text{ g}^{-1}$  by KOH (with mass ratio of KOH: Carbonized KF = 5:1) activation at  $700^\circ\text{C}$  for 2 h [26]. Wang et al. directly pyrolyzed the NaOH pre-treated kapok fibers at  $750^\circ\text{C}$  for 1 h and obtained porous carbons with a SSA of  $1126 \text{ m}^2 \text{ g}^{-1}$  [27]. Both kinds of porous carbons exhibited excellent electrochemical capacitance in aqueous electrolyte although their specific surface areas and pore volumes are inferior to many other biomass-derived porous carbons. The low texture values of the KF-derived porous carbons might be originated from the complex constituents of the raw kapok fibers including cellulose, lignin, xylan, and wax [28]. The waxy coating is especially harmful to the preparation of porous carbons because it produces a hydrophobic surface that prevents the kapok fibers from being completely wetted by the activating reagent. In the above mentioned works,  $\text{NaClO}_2$  and NaOH have been used to dewax the kapok fibers, but the waxy coating layer might be not completely removed under such mild conditions.

Herein, a low-temperature pre-carbonization step in air in combination with KOH activation was proposed to prepare highly mesoporous carbon flakes from kapok fibers (denoted as highly mesoporous carbon flakes, HMCFs). A pre-carbonization at  $300^\circ\text{C}$  in air effectively dewaxed the kapok fibers, which in turn promoted the wetting of the carbon precursor by KOH solution. With the mass ratios of 1 and 2 (KOH to the pre-carbonized precursor), the HMCFs showed specific surface areas of 2467 and  $3010 \text{ m}^2 \text{ g}^{-1}$ , and pore volumes of 1.819 and  $2.756 \text{ cm}^3 \text{ g}^{-1}$ , respectively. As will be shown, the HMCFs exhibited quite high specific energy density even at high power density, namely  $24 \text{ Wh kg}^{-1}$  at  $24,029 \text{ W kg}^{-1}$  (based on the active mass of both electrodes) when they were used as electrode materials of EDLCs in organic electrolyte. The detailed preparation, characterizations and electrochemical performances of the KF-derived mesoporous carbon flakes are reported.

## 2. Experimental details

### 2.1. Preparation and characterizations of HMCFs

The HMCFs were prepared from kapok fibers collected from Kah Kee park in Jimei district of Xiamen city, Fujian, China. The washed kapok fibers were pre-carbonized in air at  $300^\circ\text{C}$  for 2 h in a muffle furnace, which were then grounded and mixed with potassium hydroxide (KOH) in the mass ratios of 1 or 2 with addition of an appropriate amount of water. After drying at  $80^\circ\text{C}$  completely, the mixtures held in Ni crucibles were heated at  $850^\circ\text{C}$  for 4 h in a tube furnace under the protection of high purity flowing nitrogen. The resultants were washed by diluted HCl solution (1 M) and ultrapure water repeatedly, filtered and dried at  $80^\circ\text{C}$  to obtain the HMCFs. According to the amount of the KOH activating agent used, the carbon powders were named as HMCFs-1 and HMCFs-2, respectively.

The phase and microstructures of the obtained HMCFs were examined by powder X-ray diffraction (XRD, Rigaku MiniFlex600), scanning electron microscope (SEM, Zeiss Sigma 500), and transmission electronic microscope (TEM, FEI Talos F200s). The surface functional groups of the natural and pre-carbonized kapok fibers were analyzed using a Fourier-transform infrared spectrometer (FTIR, Bruker Alpha-T). The texture properties of the HMCFs were evaluated by nitrogen adsorption/desorption measurements at  $77 \text{ K}$  with a surface area and porosimetry analyzer (Micromeritics ASAP 2020 Plus). The Brunauer–Emmett–Teller (BET) method and t-plot method were used to calculate the specific surface areas and micropore volumes ( $V_{\text{mic}}$ ), respectively. The total pore volumes ( $V_t$ ) were calculated from the amount of adsorbed nitrogen at a relative pressure ( $P/P_0$ ) of 0.95. The pore size distributions within the HMCFs were estimated by the quenched solid density functional theory (QSDFT) from the adsorption branches of the nitrogen adsorption/desorption isotherms.

### 2.2. Electrochemical tests

The energy storage performances of the HMCFs were evaluated using coin-type symmetric electrochemical double layer capacitors. To prepare the electrodes, the prepared HMCFs, conductive carbon (Super C65, Timcal), and polytetrafluoroethylene (PTFE) binder (Dakin, Japan) were mixed with a weight ratio of 80:10:10 in ethanol and hand ground until stick mixtures were obtained. The mixtures were repeatedly rolled and finally pressed onto a piece of carbon-coated aluminum foil under 30 MPa, followed by drying at  $80^\circ\text{C}$  overnight in an air-blowing oven. Disk-type electrodes of 12 mm in diameter were punctured out and two of them with similar mass loading of active materials (HMCFs, about  $1–2 \text{ mg cm}^{-2}$ ) were subjected to assemble of 2025 coin-type symmetric supercapacitors. The separator and electrolyte were cellulose fibrous paper (NKKTF4030, Japan) and 1 M tetraethyl ammonium tetrafluoroborate (TEABF<sub>4</sub>) dissolved in propylene carbonate (PC), respectively. The electrochemical performances of the supercapacitors were evaluated by both cyclic voltammetry (CV) and galvanostatic charge/discharge (GCD) measurements using an electrochemical workstation (CHI660e, Chenhua, Shanghai) within a voltage range of 0–2.6 V. The cycling lives were measured at  $1 \text{ A g}^{-1}$  using a Land battery tester (CT2001A, Wuhan Kingnuo Electronic Co., China) for 5000 times. The resistances of the electrodes associated to the electrochemical reactions were examined by electrochemical impedance spectroscopy (EIS) measurements performed on an electrochemical workstation (PARSTAT™ MC, AMETEK, USA). The examined frequency range was 100 kHz to 10 mHz, and the measurements were carried out at the open circuit voltage by applying a bias of 10 mV. The specific capacitances of the cells ( $C_{\text{cell}}$ ) and electrodes ( $C_{\text{sp}}$ ) were estimated using formulas (1) and (2), respectively.

$$C_{\text{cell}} = (I\Delta t)/(mV) \quad (1)$$

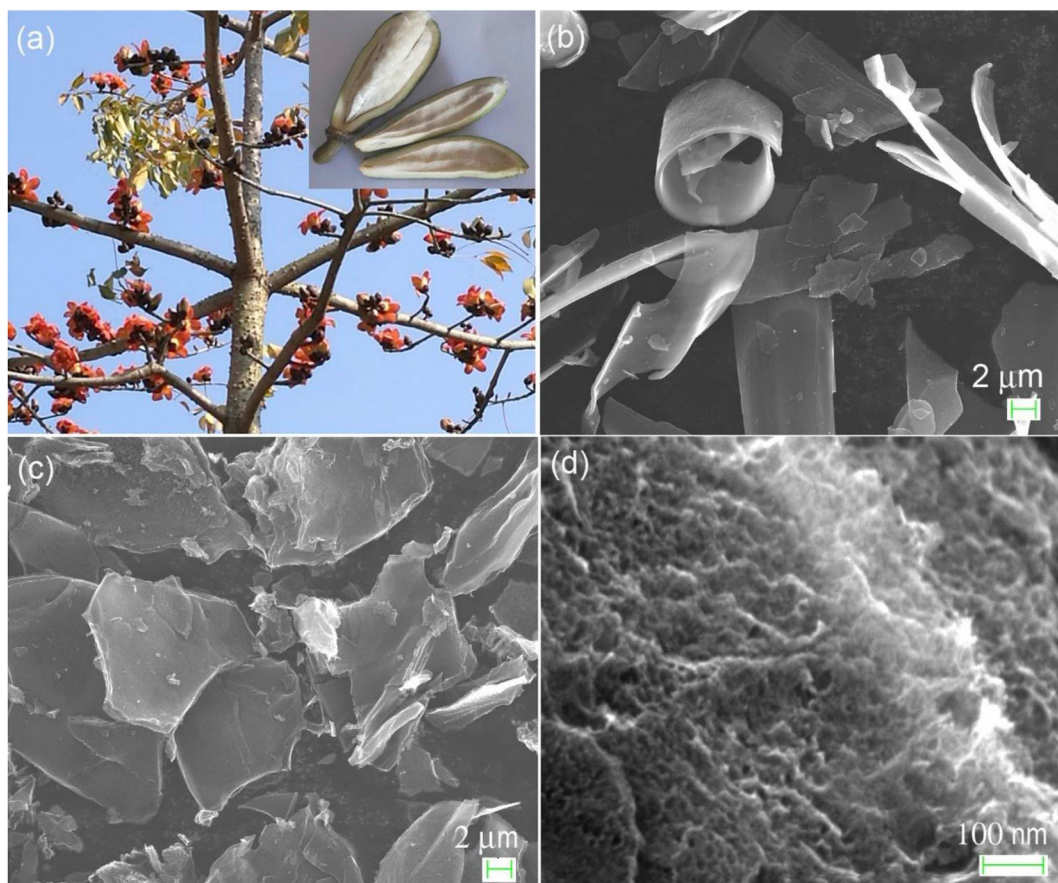


**Fig. 1.** Digital photograph of a flowering kapok tree and one broken kapok fruit (a), SEM images of the kapok fibers directly carbonized at 850 °C (b), and the activated kapok fibers (c and d) with a KOH mass ratio of 2 to the pre-carbonized kapok fibers.

$$C_{sp} = 4 * C_{cell} \quad (2)$$

Where  $I$  (A) was the discharge current,  $V$  (V) was the voltage window after deduction of the  $IR$  drop,  $\Delta t$  (s) was the discharge time, and  $m$  (g) was the mass sum of active materials in both electrodes.

The specific energy density and power density of the supercapacitor cells were calculated using formulas (3) and (4).

$$E = 0.5 * C_{cell} V^2 / 3.6 \quad (3)$$

$$p = E / \Delta t \quad (4)$$

Where  $V$  (V) was the voltage window after deduction of the  $IR$  drop, and  $\Delta t$  (h) was the discharge time.

### 3. Results and discussion

#### 3.1. Characterizations of the HMCFs

Kapok is a tropical tree of the order Malvales and the family Malvaceae, which is normally cultivated for the seed fibers, particularly in south-east Asia. In south China kapok is also planted for urban landscaping. Fig. 1a shows a digital photograph of a flowering kapok tree in a local park. The photo of one broken kapok fruit is shown in Fig. 1a inset. The kapok fibers directly carbonized at 850 °C show tubular structure with thin walls (Fig. 1b), consistent to the results of recent reports [26]. After re-carbo and KOH activation, the tubular fibers were broken into flakes with planar dimensions of mostly less than 20 μm, see Fig. 1c. Seeing more closely to the surface of the carbon flakes (Fig. 1d), porous structure with abundant nanopores was obviously observed. Such a highly porous structure can be ascribed to the

comprehensive activating effects of KOH, including the chemical activation by potassium containing compounds, the physical activation by the generated H<sub>2</sub>O and CO<sub>2</sub> gases, and the intercalation of metallic K in the carbon lattice [7]. The FTIR spectra of both the natural and the pre-carbonized kapok fibers shown in Fig. S1 clearly indicate that the natural kapok fibers have several additional peaks related to wax as compared to that of the pre-carbonized sample [29]. This demonstrates that the pre-carbonization treatment was very effective to decompose the functional groups of wax in natural kapok fibers, which improved the wetting effect of the precursor by KOH solution. It is believed that the good wetting of the two-dimensional precursor by KOH might have especially strengthened the activating effect, yielding the highly mesoporous carbon flakes.

To further examine the porous structure of the HMCFs, TEM observations were performed in both bright field and HADDF modes on HMCFs-2, as shown in Fig. 2. From the bright-field TEM image (Fig. 2a), one can clearly observe the highly porous structure of the thin carbon flakes. A HADDF image shown in Fig. 2b also reveals the existence of a large amount of nanopores in a wide range of pore sizes. The pore walls are very thin, resulting in an interconnected porous structure. The high resolution TEM image (Fig. 2c) displays highly disordered structure, indicating the amorphous nature of the obtained carbon flakes. The XRD patterns of both samples (Fig. 2d) further confirm the highly amorphous structure of the obtained carbon materials.

The degree of graphitization of the HMCFs was characterized by Raman spectra, as shown in Fig. 3a. There are two obvious peaks at 1331 cm<sup>-1</sup> and 1581 cm<sup>-1</sup>, respectively. The peak at 1331 cm<sup>-1</sup> (D) is related to defects and disorder, whereas the peak at 1581 cm<sup>-1</sup> (G) comes from the graphitic structure [30]. The intensity ratios of D band

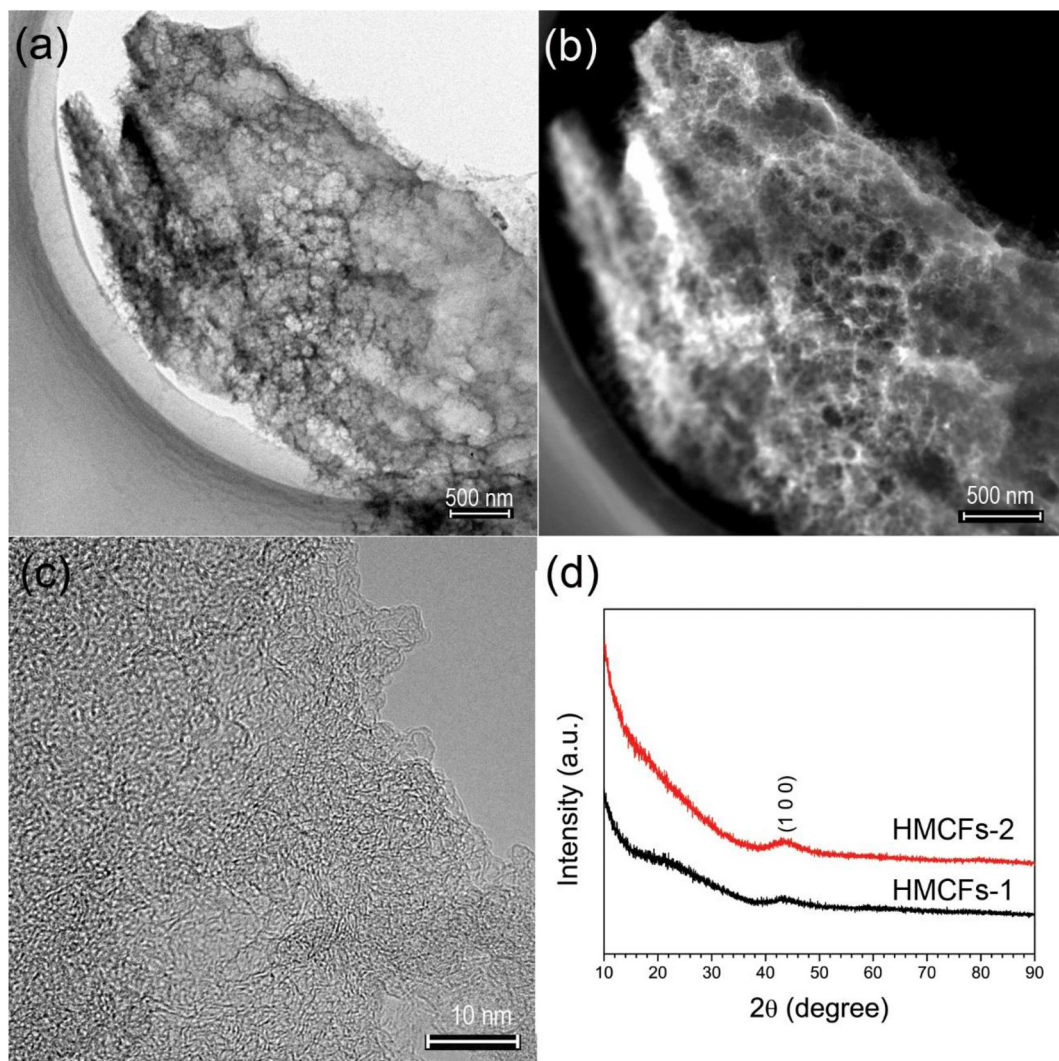


**Fig. 2.** Bright-field TEM image (a), HADDF image (b) and high resolution TEM image (c) of HMCFs-2, and XRD patterns of both samples (d).

to G band ( $I_D/I_G$ ) represent the degree of graphitization, which are 1.33 and 1.45 for HMCFs-1 and HMCFs-2, respectively. This indicates that both carbon samples are highly amorphous. The porous carbon prepared with higher mass ratio of KOH possesses lower degree of graphitization. The surface chemical compositions of the obtained carbon flakes were characterized by XPS spectra. Fig. 3b shows the XPS spectra of C1s core scan. The survey scans of both samples are depicted in Fig. 3b inset. Unlike the results of recent reports [26,27], the KOH activated kapok fibers do not show the presence of N1s signal even in a detailed N1s core scan (see Fig. S2). By contrast, the directly pyrolyzed kapok fibers did show a weak N1s peak in the XPS spectrum (Fig. S2). This demonstrated that the N-containing group in the kapok fibers was unstable under KOH activation at high temperature, resulting in N-free porous carbons. The C1s spectra can be deconvoluted into three component peaks, corresponding to C-C (284.6 eV), C-O (285.7 eV) and O-C=O (289.7 eV), respectively, indicating the presence of oxygen containing groups [15,30].

The nitrogen adsorption/desorption isotherms measured at 77 K and the pore size distributions calculated using the QSDFT model are given in Fig. 3c and d, respectively. The corresponding texture properties of both carbon samples are given in Table 1. As can be seen in Fig. 3c, the isotherms of both carbon samples can be seen as a mixture of type I and type IV isotherms according to the IUPAC classification [31]. The sharp increase of the  $N_2$  adsorption at low  $P/P_0$  is a sign of the microporous

structure, whereas the continuously increased  $N_2$  adsorption along with the increase of  $P/P_0$ , especially the appearance of hysteresis loop between the adsorption and desorption branches, clearly reveals the existence of a large amount of mesopores. As it is shown in Table 1, the BET SSA of HMCFs-1 and HMCFs-2 are  $2467$  and  $3010\text{ m}^2\text{ g}^{-1}$ , with the corresponding total pore volumes of  $1.819$  and  $2.756\text{ cm}^3\text{ g}^{-1}$ , respectively. The ratios of the micropore volumes in HMCFs-1 and HMCFs-2 as determined by the t-pot method are only 31.6% and 2.4%, respectively. This evidently demonstrates that the porous carbon flakes derived from kapok fibers are highly mesoporous. HMCFs-2 shows much higher ratio of mesopores in the total pore volume than that of HMCFs-1. Moreover, the mean pore diameter of HMCFs-2 is  $3.64\text{ nm}$ , higher than that of HMCFs-1,  $2.94\text{ nm}$ . This indicates that more adequate etching of the kapok fibers might have occurred at a higher mass loading of KOH activating reagent. The pore size distributions of both samples shown in Fig. 3d also demonstrate that HMCFs-2 possesses higher portion of mesopore volume and larger pore diameter. Such a mesopore-dominant microstructure is expected to provide sufficient channels for the diffusion of electrolyte ions, especially for organic electrolytes.

To examine the effect of other factors such as activation temperature and mass ratio on the texture properties of porous carbons, carbon samples were also prepared with KOH mass ratios of 0.5 and 3, or keeping the mass ratio of 2 but decreasing the activation temperature to

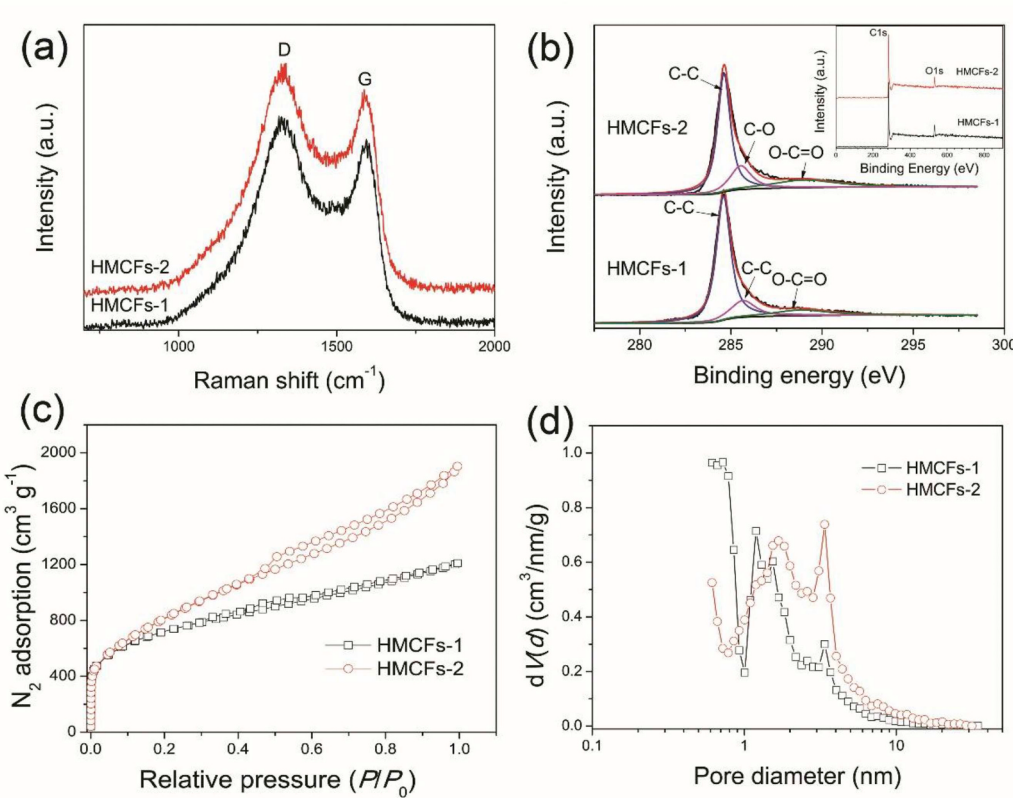


**Fig. 3.** Raman spectra (a), XPS C1s core scan (b),  $N_2$  adsorption/desorption isotherms measured at 77 K (c) and the pore size distribution (d) of the carbon flakes.

**Table 1**

The texture properties of the highly mesoporous carbon flakes derived from kapok fibers.

Sample	$S_{\text{BET}}$ ( $\text{m}^2 \text{g}^{-1}$ )	$S_{\text{mic}}$ ( $\text{m}^2 \text{g}^{-1}$ )	$V_t$ ( $\text{cm}^3 \text{g}^{-1}$ )	$V_{\text{mic}}$ ( $\text{cm}^3 \text{g}^{-1}$ )	$V_{\text{mic}}/V_t$	$D_{\text{mean}}$ (nm)
HMCFs-1	2467	1189	1.819	0.575	0.316	2.94
HMCFs-2	3010	250	2.756	0.068	0.024	3.64

650 °C and 750 °C. When the mass ratios of KOH to the pre-carbonized kapok fibers were 0.5 and 3, the specific surface areas of the porous carbons were 2142 and 1832  $\text{m}^2 \text{g}^{-1}$ , respectively, see  $N_2$  adsorption isotherms shown in Fig. S3. The sharp decrease of the specific surface area for the sample with the mass ratio of 3 should be ascribed to the severe etching of the carbon matrix, which has widened the micropores and interconnected the mesopores, and resulted in the decreased surface area and pore volume. The influence of activation temperature on the  $N_2$  adsorption is compared in Fig. S4. It is evident that low activation temperature is not enough to activate the pre-carbonized kapok fibers to produce high surface area. When the activation temperature was decreased to 650 °C and 750 °C, the specific surface areas of the obtained porous carbons were only 1281 and 1982  $\text{m}^2 \text{g}^{-1}$ , respectively. It is clear that the two carbon samples reported in this manuscript can represent the superior specific surface area and pore structure of the kapok fibers derived porous carbon flakes. So the electrochemical capacitance of these two samples are systematically measured.

### 3.2. Electrochemical performances

The electrochemical performances of the obtained HMCFs were evaluated by two-electrode symmetrical supercapacitors using 1 M TEABF<sub>4</sub>/PC electrolyte. Fig. 4a and b shows the cyclic voltammetry

(CV) curves of both cells measured at 10 and 500  $\text{mV s}^{-1}$  respectively. Both cells show well-preserved rectangular CV curves even at 500  $\text{mV s}^{-1}$ , demonstrating their good capacitive energy storage behaviors and rate capabilities. Cell HMCFs-2 shows obviously larger area of CV scan than HMCFs-1, consistent to its larger surface area and pore volume. This means that HMCFs-2 possesses higher capacitance than HMCFs-1. The charge and discharge curves of both cells at a constant current density of 0.2  $\text{A g}^{-1}$  are displayed in Fig. 4c. Both cells show triangle shape GCD curves, which again illustrates the good double layer charge storage mechanism. Cell HMCFs-2 exhibits a discharge capacitance of 144  $\text{F g}^{-1}$ , which is higher than that of cell HMCFs-1, 133  $\text{F g}^{-1}$ . The higher capacitance of HMCFs-2 can be correlated to its higher specific surface area and more mesoporous structure. According to Keh and Chen [32], the motion of colloidal sphere in a smaller pore will encounter a larger resistance. For the organic electrolyte ions of TEA<sup>+</sup>/BF<sub>4</sub><sup>-</sup> with relatively large size, mesopores are more accessible than micropores because of their less resistance to the transportation of ions. The ultrahigh fraction of mesopores in HMCFs-2 is likely one of the major reasons for the enhanced capacitance and also smaller IR drop in the supercapacitor cells as will be discussed shortly.

The typical charge-discharge curves of both cells measured at current densities of 10 and 20  $\text{A g}^{-1}$  with marked IR drops are displayed in Fig. 4d. The supercapacitors assembled by the highly mesoporous carbon flakes derived from kapok fibers exhibit obviously smaller IR drops as compared to that assembled by microporous carbon spheres reported in our previous publication [33]. For example, the IR drops of cell HMCFs-1 and cell HMCFs-2 at 10  $\text{A g}^{-1}$  are only 0.12 and 0.25 V, respectively. However, the IR drop of the cell assembled by microporous carbon spheres is 0.33 V at 5  $\text{A g}^{-1}$  [33]. This clearly hints that the highly mesoporous carbon flakes are beneficial to promote the transportation of electrolyte ions and reduce the inner resistance due to the increased contact area between the carbon electrode materials and electrolyte. From Fig. 4d, we can further identify that, with larger

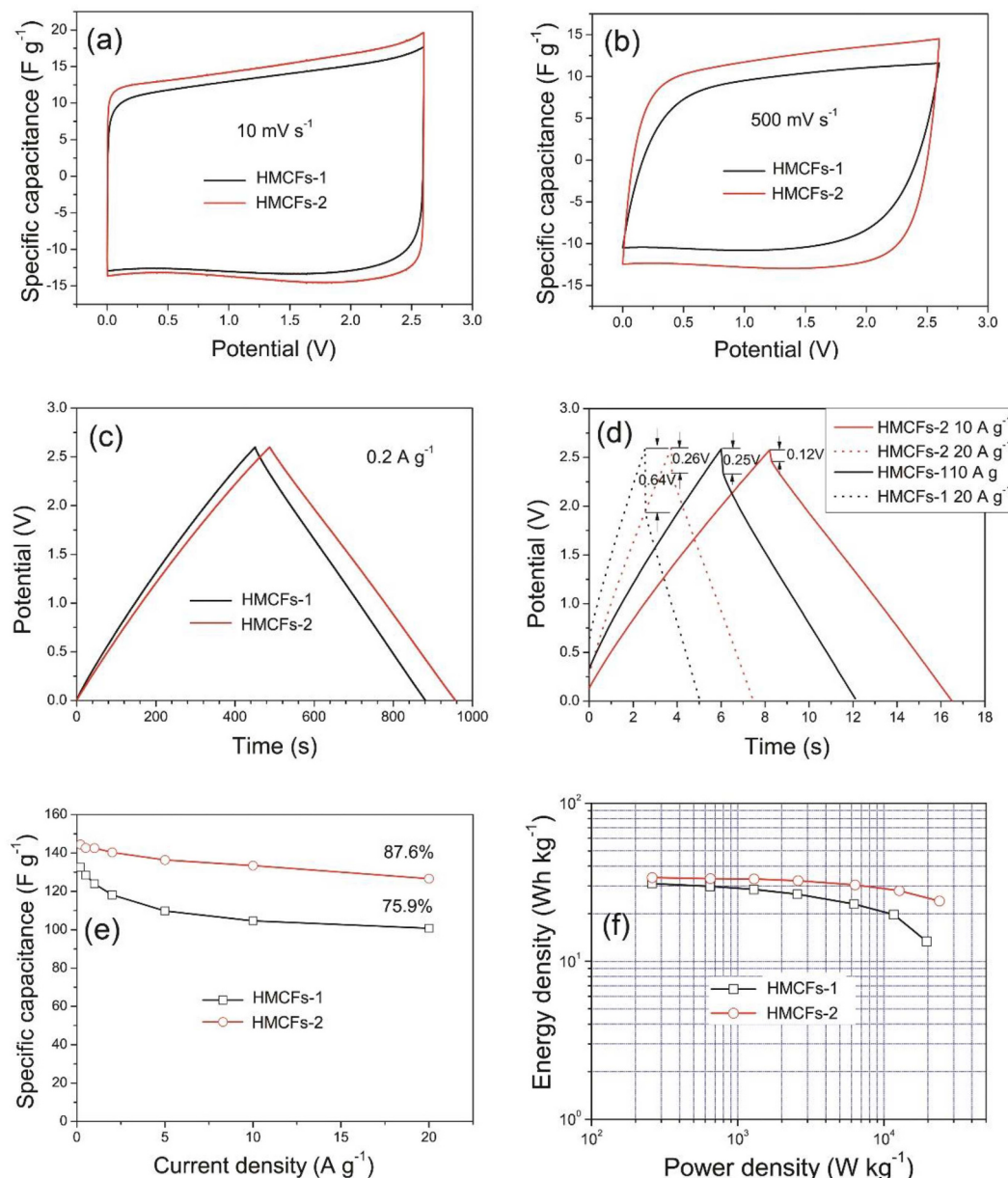


**Fig. 4.** The electrochemical performances of the symmetrical supercapacitors made of the HMCFs-1 and HMCFs-2 electrodes, CV curves measured at (a)  $10 \text{ mV s}^{-1}$  and (b)  $500 \text{ mV s}^{-1}$ , GCD curves measured at  $0.2 \text{ A g}^{-1}$  (c) and at  $10$  and  $20 \text{ A g}^{-1}$  (d), rate capability (e) and ragone plots (f).

mesoporevolume and pore size, cell HMCFs-2 shows further reduced *IR* drop as compared to cell HMCFs-1. This illustrates that cell HMCFs-2 possess better rate performance, as confirmed in Fig. 4e. The specific capacitances of cell HMCFs-2 at current densities of 0.2, 0.5, 1, 2, 5, 10 and  $20 \text{ A g}^{-1}$  are 144, 143, 142, 140, 136, 133, and  $127 \text{ F g}^{-1}$ , respectively. The corresponding data for cell HMCFs-1 are 133, 129, 124, 118, 110, 105 and  $101 \text{ F g}^{-1}$ , respectively. The capacitance retentions of HMCFs-1 and HMCFs-2 at  $20 \text{ A g}^{-1}$  are 75.9% and 87.6% respectively of those at  $0.2 \text{ A g}^{-1}$ . These capacitances clearly reveal that the rate performance of the carbon materials can be greatly improved by introducing more mesopores and widening the pore size. Fig. 4f displays the ragone plots of both supercapacitors. Cells HMCFs-1 and HMCFs-2 show energy densities of 31 and  $33.8 \text{ Wh kg}^{-1}$  respectively at a power density of  $260 \text{ W kg}^{-1}$ . The capacitance difference between these two cells is not so significant at low power density. However, with the increase of power density, the energy density of cell HMCFs-1 drops much faster than that of cell HMCFs-2. For example, the latter cell

can still deliver an energy density of  $24 \text{ Wh kg}^{-1}$  at a power density of  $24,029 \text{ W kg}^{-1}$ , whereas the energy density of cell HMCFs-1 is only  $13.3 \text{ Wh kg}^{-1}$  at a power density of  $19,635 \text{ W kg}^{-1}$ . The specific energy density of cell HMCFs-2 is among the best values reported recently on biomass-derived carbon-based EDLCs in organic electrolyte, as compared in Table 2.

The cycle performances of both supercapacitors were measured at  $1 \text{ A g}^{-1}$  for 5000 cycles, as shown in Fig. 5a. Cells HMCFs-1 and HMCFs-2 retain 88% and 91% of their initial capacitances after 5000 cycles. Although cell HMCFs-2 show inferior capacitance retention than cell HMCFs-1, it can maintain a specific capacitance of  $130 \text{ F g}^{-1}$  after 5000 cycles. This indicates that the highly mesoporous carbon flakes derived from kapok fibers can be potentially used as electrode materials of EDLCs with high capacitance. It is well known that the mesopores can help to increase the contact area of electrolyte and electrode, and facilitate the transportation of electrolyte ions. In other words, the mesoporous structure might have increased the accessible surface area

**Table 2**

Comparison of biomass-derived carbon materials for EDLCs in organic electrolyte.

Carbon samples	Electrolyte	Power density (kW kg <sup>-1</sup> )	Energy density (Wh kg <sup>-1</sup> )	Ref.
Silkworm cocoon	1 M TEABF <sub>4</sub> /AN	3.12	34.4	[34]
Pomelo peels	1 M TEABF <sub>4</sub> /PC	21.5	25.3	[35]
Peanut shell	1 M Et <sub>4</sub> NBF <sub>4</sub> /PC	1.0	19.3	[36]
Hemp stem	1.8 M TEABF <sub>4</sub> /PC	21	19.8	[37]
Tobacco rods	1 M CH <sub>3</sub> (C <sub>2</sub> H <sub>5</sub> ) <sub>3</sub> NBF <sub>4</sub> /AN	15 A g <sup>-1</sup>	11.8	[38]
Leonardite fulvic acid	1 M TEABF <sub>4</sub> /PC	5.89	23.3	[39]
Pollens	1 M TEABF <sub>4</sub> /AN	46	1 A g <sup>-1</sup>	[40]
Lignin/hemicellulose	1 M TEABF <sub>4</sub> /AN			[41]
Paper pulp	1 M TEABF <sub>4</sub> /AN	20	5.45	[42]
YP-50F (Kuraray)	1 M TEABF <sub>4</sub> /PC	7.095	4.5	[33]
Kapok fibers	1 M TEABF <sub>4</sub> /PC	0.26	33.8	This work
		24	24	This work

of electrode materials. The electrochemical impedance spectra of both cells were measured after the cycling tests and the Nyquist plots are shown in Fig. 5b. Both Nyquist plots show an almost vertical line in low-frequency range, which demonstrates an ideal capacitive behavior in both cells. The equivalent series resistance (ESR) of cells HMCFs-1 and HMCFs-2, as obtained by extrapolating the vertical portion of the plot to the real axis, are about 9 and 8.2 Ω, respectively. By fitting the impedance spectra using the Zview software, cell HMCFs-2 also shows smaller charge transfer resistance (7.6 Ω) than cell HMCFs-1 (8.6 Ω) owing to its larger mesopore volume and pore size. The relaxation time constants,  $\tau_0$ , as were deduced from  $\tau_0 = 1/f_0$  ( $f_0$  is obtained from the

real capacitance plot at  $C'/C'_{\max} = 0.5$  [43]) for cells HMCFs-1 and HMCFs-2, are 3.38 and 1.75 S, respectively (see Fig. 5c). It is known that the relaxation time constant define the boundary between the regions of capacitive and resistive behaviors of the supercapacitors. Cell HMCFs-2 exhibits clearly shorter responding time, which is consistent to its better energy storage capabilities. The  $f_0$  of cell HMCFs-2 determined from the variation of the imaginary capacitance with frequency (Fig. 5d) is also higher than that of cell HMCFs-1, indicative of its lower maximum energy dissipation. The above electrochemical performances indicate that the KF-derived porous carbon flakes with higher portion of mesopore volume, larger surface area and pore size might be the ideal candidate electrode materials of EDLCs.

#### 4. Conclusions

Highly mesoporous carbon flakes were prepared by pre-carbonization and KOH activation of tubular kapok fibers. As compared to reference works, an ultrahigh specific surface area of 3010 m<sup>2</sup> g<sup>-1</sup> and a very large pore volume of 2.756 cm<sup>3</sup> g<sup>-1</sup> were obtained with a mass ratio of 2 (KOH to the pre-carbonized precursor). Moreover, the carbon sample shows a mesopore volume ratio of as high as 97.6%. Such a highly mesoporous structure enables the carbon flakes to be promising electrode materials of EDLCs in organic electrolyte. For an optimum case, energy densities of 33.8 and 24 Wh kg<sup>-1</sup> were measured at power densities of 260 and 24,029 W kg<sup>-1</sup>, respectively, which were among the best values reported so far on biomass-derived carbon electrode materials. The results reported here hint that by combination of pre-carbonization, use of two-dimensional precursors and KOH activation, highly porous carbon flakes or nanosheets with high volume ratio of mesopores can be obtained, which opens up a versatile way to monitor the texture properties of biomass-derived carbonaceous electrode materials for EDLCs with enhanced capacitive performance.

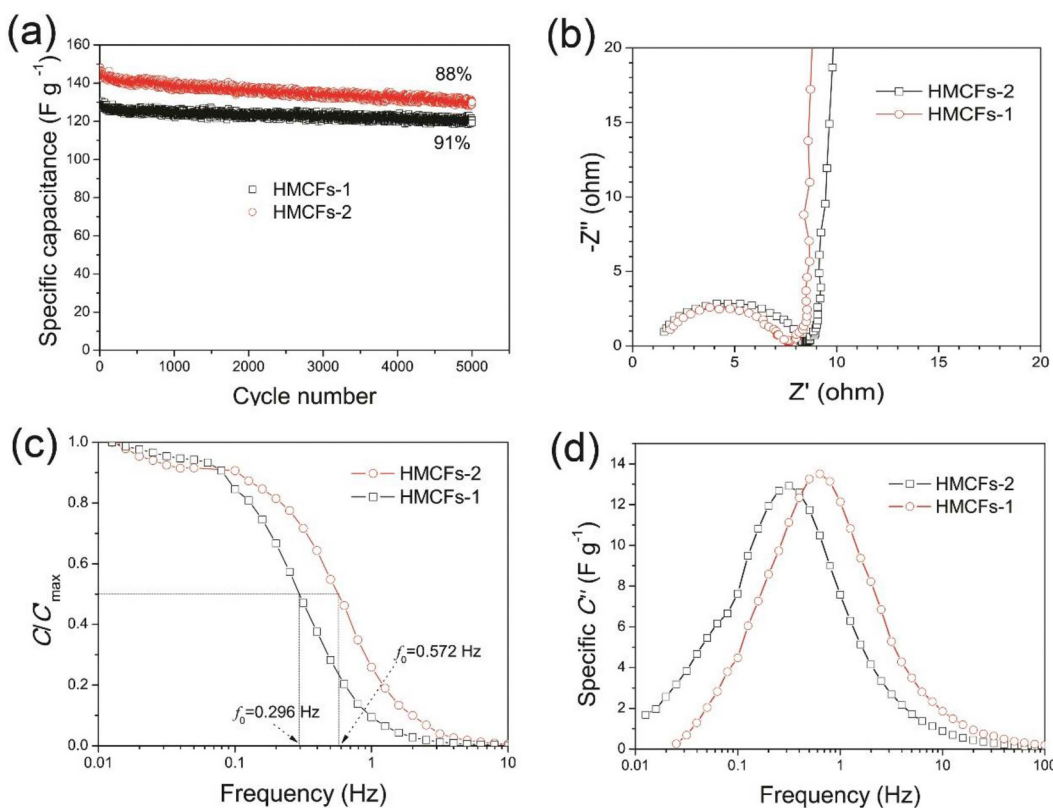


**Fig. 5.** (a) The cycle performances of the supercapacitors assembled with the HMCFs-1 and HMCFs-2 electrodes measured at 1 A g<sup>-1</sup>, (b) the Nyquist plots, (c) the frequency dependence of the normalized real part capacitance and (d) the specific capacitance of the imaginary part of the corresponding cells after the cycling tests.

## Acknowledgements

The authors gratefully acknowledge the financial supports from the Natural Science Foundation project (No. 2016J01746) and Guidance Project of Fujian Province, China (No. 2016H0038), Open Project of Key Laboratory of Environmental Biotechnology (XMUT) (No. EBL2018007), and Program for Innovative Research Team in Science and Technology in Fujian Province University.

## Appendix A. Supplementary data

Supplementary data to this article can be found online at <https://doi.org/10.1016/j.matchemphys.2018.10.036>.

## References

- [1] E. Frackowiak, Q. Abbas, F. Béguin, Carbon/carbon supercapacitors, *J. Energy Chem.* 22 (2013) 226–240.
- [2] Y. Wang, Y. Song, Y. Xia, Electrochemical capacitors: mechanism, materials, systems, characterization and applications, *Chem. Soc. Rev.* 45 (2016) 5925–5950.
- [3] Q. Li, X. Guo, Y. Zhang, W. Zhang, C. Ge, L. Zhao, X. Wang, H. Zhang, J. Chen, Z. Wang, L. Sun, Porous graphene paper for supercapacitor applications, *J. Mater. Sci. Technol.* 33 (2017) 793–799.
- [4] T. Chen, L. Dai, Carbon nanomaterials for high-performance supercapacitors, *Mater. Today* 16 (2013) 272–280.
- [5] Q. Wang, J. Yan, Z. Fan, Carbon materials for high volumetric performance supercapacitors: design, progress, challenges and opportunities, *Energy Environ. Sci.* 9 (2016) 729–762.
- [6] J. Wang, M. Chen, C. Wang, J. Wang, J. Zheng, Preparation of mesoporous carbons from amphiphilic carbonaceous material for high-performance electric double-layer capacitors, *J. Power Sources* 196 (2011) 550–558.
- [7] J. Wang, S. Kaskel, KOH activation of carbon-based materials for energy storage, *J. Mater. Chem.* 22 (2012) 23710–23725.
- [8] C. Jiang, J. Zhang, Nanoengineering titania for high rate lithium storage: a review, *J. Mater. Sci. Technol.* 29 (2013) 97–122.
- [9] Y. Zhu, S. Murali, M.D. Stoller, K.J. Ganesh, W. Cai, P.J. Ferreira, A. Pirkle, R.M. Wallace, K.A. Cychosz, M. Thommes, D. Su, E.A. Stach, R.S. Ruoff, Carbon-based supercapacitors produced by activation of graphene, *Science* 332 (2011) 1537–1541.
- [10] C. Liu, Z. Yu, D. Neff, A. Zhamu, B.Z. Jang, Graphene-based supercapacitor with an ultrahigh energy density, *Nano Lett.* 10 (2010) 4863–4868.
- [11] H. Pan, J. Li, Y. Feng, Carbon nanotubes for supercapacitor, *Nanoscale Res. Lett.* 5 (2010) 654.
- [12] W. Tang, Y. Zhang, Y. Zhong, T. Shen, X. Wang, X. Xia, J. Tu, Natural biomass-derived carbons for electrochemical energy storage, *Mater. Res. Bull.* 88 (2017) 234–241.
- [13] L. Jiang, L. Sheng, Z. Fan, Biomass-derived carbon materials with structural diversities and their applications in energy storage, *Sci. Chin. Mater.* 61 (2018) 133–158.
- [14] D. A, S.A.B.A. Manaf, Y. S, C. K, K. N, G. Hegde, Low cost, high performance supercapacitor electrode using coconut wastes: eco-friendly approach, *Journal of Energy Chemistry* 25 (2016) 880–887.
- [15] H. Wang, Z. Xu, A. Kohandehghan, Z. Li, K. Cui, X. Tan, T.J. Stephenson, C.K. King'ondu, C.M.B. Holt, B.C. Olsen, J.K. Tak, D. Harfield, A.O. Anyia, D. Mitlin, Interconnected carbon nanosheets derived from hemp for ultrafast supercapacitors with high energy, *ACS Nano* 7 (2013) 5131–5141.
- [16] J. Hou, C. Cao, F. Idrees, X. Ma, Hierarchical porous nitrogen-doped carbon nanosheets derived from silk for ultrahigh-capacity battery anodes and supercapacitors, *ACS Nano* 9 (2015) 2556–2564.
- [17] L. Pang, B. Zou, X. Han, L. Cao, W. Wang, Y. Guo, One-step synthesis of high-performance porous carbon from corn starch for supercapacitor, *Mater. Lett.* 184 (2016) 88–91.
- [18] W. Tian, Q. Gao, L. Zhang, C. Yang, Z. Li, Y. Tan, W. Qian, H. Zhang, Renewable graphene-like nitrogen-doped carbon nanosheets as supercapacitor electrodes with integrated high energy-power properties, *J. Mater. Chem.* 4 (2016) 8690–8699.
- [19] Y.S. Yun, M.H. Park, S.J. Hong, M.E. Lee, Y.W. Park, H.-J. Jin, Hierarchically porous carbon nanosheets from waste coffee grounds for supercapacitors, *ACS Appl. Mater. Interfaces* 7 (2015) 3684–3690.
- [20] L. Zhang, T. You, T. Zhou, X. Zhou, F. Xu, Interconnected hierarchical porous carbon from lignin-derived byproducts of bioethanol production for ultra-high performance supercapacitors, *ACS Appl. Mater. Interfaces* 8 (2016) 13918–13925.
- [21] W. Yu, H. Wang, S. Liu, N. Mao, X. Liu, J. Shi, W. Liu, S. Chen, X. Wang, N. O-codoped hierarchical porous carbons derived from algae for high-capacity supercapacitors and battery anodes, *J. Mater. Chem.* 4 (2016) 5973–5983.
- [22] W. Tian, Q. Gao, Y. Tan, Z. Li, Unusual interconnected graphitized carbon nanosheets as the electrode of high-rate ionic liquid-based supercapacitor, *Carbon* 119 (2017) 287–295.
- [23] K. Wang, N. Zhao, S. Lei, R. Yan, X. Tian, J. Wang, Y. Song, D. Xu, Q. Guo, L. Liu, Promising biomass-based activated carbons derived from willow catkins for high performance supercapacitors, *Electrochim. Acta* 166 (2015) 1–11.
- [24] C. Peng, X.-b. Yan, R.-t. Wang, J.-w. Lang, Y.-j. Ou, Q.-j. Xue, Promising activated carbons derived from waste tea-leaves and their application in high performance supercapacitors electrodes, *Electrochim. Acta* 87 (2013) 401–408.
- [25] E.Y.L. Teo, L. Muniandy, E.-P. Ng, F. Adam, A.R. Mohamed, R. Jose, K.F. Chong, High surface area activated carbon from rice husk as a high performance supercapacitor electrode, *Electrochim. Acta* 192 (2016) 110–119.
- [26] W. Xu, B. Mu, A. Wang, Porous carbon nanoflakes with a high specific surface area derived from a kapok fiber for high-performance electrode materials of supercapacitors, *RSC Adv.* 6 (2016) 6967–6977.
- [27] J.-R. Wang, F. Wan, Q.-F. Lü, F. Chen, Q. Lin, Self-nitrogen-doped porous biochar derived from kapok (*Ceiba insignis*) fibers: effect of pyrolysis temperature and high electrochemical performance, *J. Mater. Sci. Technol.* 34 (2018) 1959–1968.
- [28] Y. Liu, J. Wang, Y. Zheng, A. Wang, Adsorption of methylene blue by kapok fiber treated by sodium chloride optimized with response surface methodology, *Chem. Eng. J.* 184 (2012) 248–255.
- [29] R.S. Rengasamy, D. Das, C. Praba Karan, Study of oil sorption behavior of filled and structured fiber assemblies made from polypropylene, kapok and milkweed fibers, *J. Hazard. Mater.* 186 (2011) 526–532.
- [30] W. Tian, Q. Gao, Y. Tan, Y. Zhang, J. Xu, Z. Li, K. Yang, L. Zhu, Z. Liu, Three-dimensional functionalized graphenes with systematical control over the interconnected pores and surface functional groups for high energy performance supercapacitors, *Carbon* 85 (2015) 351–362.
- [31] J. Rouquerol, D. Avnir, C.W. Fairbridge, D.H. Everett, J.M. Haynes, N. Pernicone, J.D.F. Ramsay, K.S.W. Sing, U. KK, Recommendations for the characterization of porous solids (Technical Report), *Pure Appl. Chem.* 66 (1994) 1739–1758.
- [32] H.J. Keh, S.B. Chen, Diffusiophoresis and electrophoresis of colloidal cylinders, *Langmuir* 9 (1993) 1142–1149.
- [33] Z. Zou, J. Zhao, J. Xue, R. Huang, C. Jiang, Highly porous carbon spheres prepared by boron-templating and reactive H<sub>3</sub>PO<sub>4</sub> activation as electrode of supercapacitors, *J. Electroanal. Chem.* 799 (2017) 187–193.
- [34] J. Sun, J. Niu, M. Liu, J. Ji, M. Dou, F. Wang, Biomass-derived nitrogen-doped porous carbons with tailored hierarchical porosity and high specific surface area for high energy and power density supercapacitors, *Appl. Surf. Sci.* 427 (2018) 807–813.
- [35] F. Sun, L. Wang, Y. Peng, J. Gao, X. Pi, Z. Qu, G. Zhao, Y. Qin, Converting biomass waste into microporous carbon with simultaneously high surface area and carbon purity as advanced electrochemical energy storage materials, *Appl. Surf. Sci.* 436 (2018) 486–494.
- [36] X. He, P. Ling, J. Qiu, M. Yu, X. Zhang, C. Yu, M. Zheng, Efficient preparation of biomass-based mesoporous carbons for supercapacitors with both high energy density and high power density, *J. Power Sources* 240 (2013) 109–113.
- [37] W. Sun, S.M. Lipka, C. Swartz, D. Williams, F. Yang, Hemp-derived activated carbons for supercapacitors, *Carbon* 103 (2016) 181–192.
- [38] Y. Zhao, M. Lu, P. Tao, Y. Zhang, X. Gong, Z. Yang, G. Zhang, H. Li, Hierarchically porous and heteroatom-doped carbon derived from tobacco rods for supercapacitors, *J. Power Sources* 307 (2016) 391–400.
- [39] Y. Ma, Y. Guo, C. Zhou, C. Wang, Biomass-derived dendritic-like porous carbon aerogels for supercapacitors, *Electrochim. Acta* 210 (2016) 897–904.
- [40] L. Zhang, F. Zhang, X. Yang, K. Leng, Y. Huang, Y. Chen, High-performance supercapacitor electrode materials prepared from various pollens, *Small* 9 (2013) 1342–1347.
- [41] W. Tian, Q. Gao, W. Qian, Interlinked porous carbon nanoflakes derived from hydrolyzed residue during cellulosic bioethanol production for ultrahigh-rate supercapacitors in nonaqueous electrolytes, *ACS Sustain. Chem. Eng.* 5 (2017) 1297–1305.
- [42] H. Wang, Z. Li, J.K. Tak, C.M.B. Holt, X. Tan, Z. Xu, B.S. Amirkhiz, D. Harfield, A. Anyia, T. Stephenson, D. Mitlin, Supercapacitors based on carbons with tuned porosity derived from paper pulp mill sludge biowaste, *Carbon* 57 (2013) 317–328.
- [43] R. Kötz, M. Carlen, Principles and applications of electrochemical capacitors, *Electrochim. Acta* 45 (2000) 2483–2498.